Int. J. Heat Mass Transfer. Vol. 20, pp. 815–826. Pergamon Press 1977. Printed in Great Britain

PREDICTION OF MULTILAYER CHIMNEY LINER TEMPERATURES UNDER UNSTEADY STATE CONDITIONS

R. G. SIDDALL
Sheffield University, Department of Chemical Engineering and Fuel Technology, Sheffield S1 3JD, U.K.

and

J. K. PEARSON
Shell Research Ltd., Thornton Research Centre, P.O. Box 1, Chester CH1 3SH, U.K.

(*Received* 19 *May* 1976 *and in revised form* 4 *June* 1976)

Abstract—A mathematical model is presented which may be used to predict the temperature at any point in a multilayer chimney under the unsteady state conditions encountered with variable inlet temperature and mass flow rate of the chimney gases, and variable ambient temperature. The model satisfactorily predicts the temperatures measured in a three-layer experimental chimney over both the heating and cooling periods of operation. In particular, the model correctly determines the period of time for which any portion of the inner chimney liner is below the acid and water dewpoint temperatures of the chimney gases. By ensuring that this time is minimized by modifications in domestic chimney design and boiler operating conditions, the tendency for acid and water condensation and the attendant chimney corrosion can be substantially reduced.

NOMENCLATURE

B, Biot number;
C, mass specific heat;
F_1, function, $\dot{m}(\tau/\beta)/\dot{m}(t)$;
F_2, function, $[\dot{m}(t)/\dot{m}(0)]^{-0.2}$;
F_3, function, $[\dot{m}(t)/\dot{m}(0)]^{+0.8}$;
F_4, function, $\phi_a(z, t)$;
h, heat-transfer coefficient;
K, thermal conductivity;
L, height of chimney;
$\dot{m}$, mass flow rate of chimney gases;
m, counter for radial position within a solid layer;
M, total number of radial increments within a solid layer;
n, counter for time steps;
r, radial distance;
R, dimensionless radial distance;
t, time;
u, gas velocity in chimney;
w, dummy variable;
y, dimensionless distance from base of chimney ($=\varepsilon z$);
z, distance from base of chimney.

Greek symbols

α, thermal diffusivity;
β, constant defined as α_1/r_4^2;
γ, function of increment lengths in the radial position–time plane;
ε, constant defined as $2h_g(0)/r_1\rho_g C_g U(0)$;
η, the product $B_g F_3(i, n+\frac{1}{2})$;
θ, temperature;
λ, ratio of thermal diffusivities (α/α_1);
ρ, density;
τ, dimensionless time $= \beta(t-t_D)$;
ϕ, dimensionless temperature $= \theta/\theta_i(0)$;
ψ, ratio of dimensionless radius and dimensionless radial step length.

Subscripts

a, ambient conditions (cooling air conditions in experimental work);
A, cooling air;
C, cooling down portion of a complete cycle;
D, retarded (or delay);
f, on the first pass;
g, chimney gas;
H, heating up portion of a complete cycle;
i, at chimney inlet;
j, ($=1, 2$ or 3) in jth solid layer;
o, at the outer solid layer–ambient air interface;
s, at the inner liner–chimney gas interface.

1. INTRODUCTION

THE DEVELOPMENT of domestic and industrial boilers with increased thermal efficiencies, and consequently lower exhaust gas temperatures, has increased the tendency for water and acid condensation to occur in conventional chimneys. Such condensation gives rise to chimney liner corrosion, the staining and gradual disintegration of internal wall surfaces and cost and inconvenience to the user. It is therefore essential to identify and avoid boiler and chimney operating conditions which might lead to condensation from the exhaust gases. To the best of the authors' knowledge, no attempt has been made to put the subject of condensation in chimneys on a firm theoretical basis.

In a typical operating cycle in a domestic heating system, the boiler is switched on from cold, the fuel ignites and the exhaust gases enter the base of the chimney. The temperature of the exhaust gases at the chimney base increases rapidly with time until it attains a steady value. The chimney temperature also increases

with time, and will be below the acid and water dewpoint temperatures for a portion of the heating period. Once sufficient heat has been supplied for domestic requirements, the burner switches off, and the mass flow of exhaust gases rapidly diminishes as does the exhaust gas temperature. Cold air moving under natural draught then replaces the exhaust gas and its mass flow rate decreases with time as the chimney cools. The chimney temperature will, for part of the cooling period, be below the acid and water dewpoint temperatures. Once a certain time has elapsed, the burner is automatically switched on and so the cycle is repeated. After several cycles have been completed the cycling pattern becomes steady and each cycle is identical.

The mathematical model described in this paper predicts the temperature of the inside of a multilayer chimney at any position during operation. The model essentially solves the unsteady state heat-conduction equation within the chimney wall and this is coupled to a differential equation describing the energy balance for gas flowing up the chimney. The resulting equations have been solved numerically. The computer output is both in the form of numerical data and also graphical, whereby the temperatures of the inner chimney liner are plotted for heating, cooling and cycling conditions. A knowledge of the acid and water dewpoint temperatures will then determine the length of time the chimney is subject to acid and water condensation for any of these conditions. No attempt has been made in this paper to estimate amounts of fluid deposited on the chimney liner.

The ultimate aim of the mathematical model is to predict actual chimney behaviour. As a first step, the model was set up to predict the behaviour of an experimental chimney and the practical measurements served to test the accuracy of the model. In this paper the model predictions have been compared with the experimental measurements made in the chimney.

2. THE EXPERIMENTAL CHIMNEY AND MEASUREMENTS MADE

Experimental tests were carried out by DOBETA (Domestic Oil Burning Equipment Testing Association) on the chimney shown in Fig. 1. Measurements were carried out over 6 ft of the 4-in I.D. steel chimney which was attached to a boiler fired on kerosene fuel. Cooling air was forced through a surrounding jacket of 7-in dia in an attempt to simulate the most severe conditions likely to be encountered in practice with high winds. These are the conditions which produce greatest condensation.

The purpose of the experimental work was to determine the input quantities required by the mathematical model and to compare the measured gas and chimney temperatures taken over a complete cycle with the corresponding predictions.

The following quantities were measured:

(i) The mass flow rate of fuel.
(ii) The concentration of carbon dioxide which determined the mass flow rate of air.

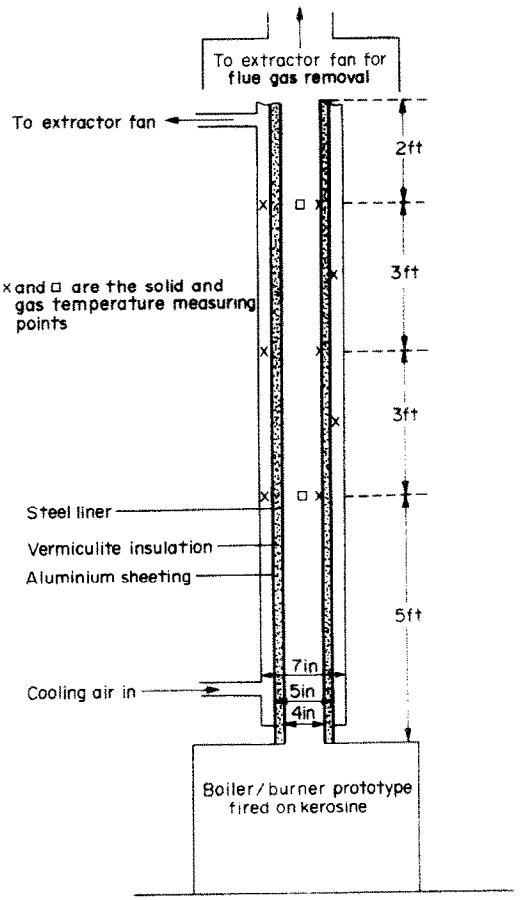

FIG. 1. Diagram of experimental chimney rig.

(iii) The velocity of the residual air flow during the cooling period.
(iv) The gas temperatures at the inlet and outlet of the test section, which were recorded continuously.
(v) The temperature of the inner liner at the top of the test section, which was recorded continuously.
(vi) Inner liner temperatures
(vii) Outer liner temperatures
(viii) Cooling air temperatures

} Measured at positions shown by x in Fig. 1 and recorded at 20-s intervals.

A typical measured inlet gas temperature vs time curve is shown in Fig. 2(a). This is taken over a complete cycle, i.e. one heating period and one cooling period. Figure 2(b) shows the corresponding curve of total mass flow rate of gas through the chimney vs time. Both these sets of information are required as input data for the mathematical model.

3. A MATHEMATICAL MODEL TO PREDICT THE EXPERIMENTAL CHIMNEY BEHAVIOUR

3.1. *Physical model and assumptions*

Figure 3 shows a cross section of a typical cylindrical three layer chimney consisting of a thin metal inner liner, a layer of insulating material and an outer layer.

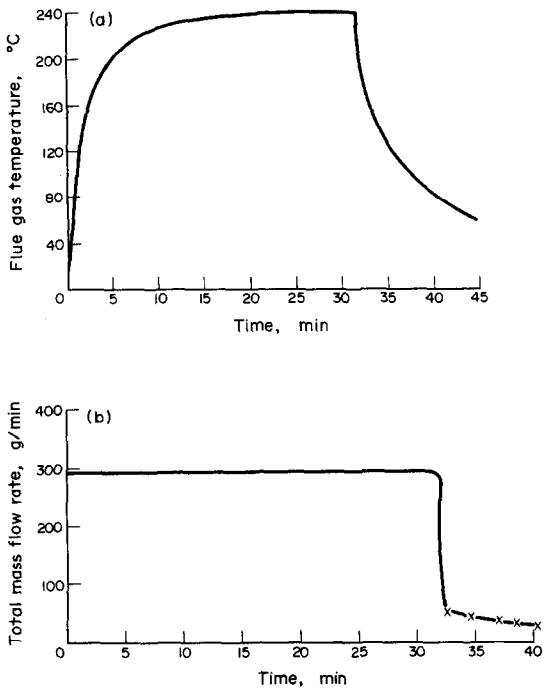

FIG. 2. Mass flow rate and temperature of flue gases vs time for Test *A* (firing rate 57.7 g/min, 12.6% CO_2).

The hot exhaust gases pass through the chimney transferring heat to the inner liner surface by convection in the heating period. An energy balance equation is required for the gas flowing up the chimney. Heat is conducted through the inner liner, the insulation and the outer layer which, in practice, loses heat by convection and radiation to the surroundings. The unsteady state heat-conduction equation applies to each of the three layers.

For the chimney under test, several physical assumptions are used in order to simplify the formulation and solution of the mathematical model. These are:

(i) As a first approximation, the effect of condensation on heat transfer is assumed to be negligible, so that the variation of liner temperature can be predicted without consideration of any mass transfer.

(ii) As it is required to study the worst conditions that can occur (from the condensation aspect), the entire chimney structure is assumed to be initially at the ambient air temperature for the first heating period, and forced convective cooling conditions are assumed for the outer face.

(iii) A linear heat loss law is assumed at the outer face of the chimney. In the case of the experimental chimney this will be true because radiation is negligible compared with convection.

(iv) On the basis of preliminary order of magnitude calculations, conduction in the z direction (i.e. along the chimney height) is neglected in comparison with radial conduction for both the chimney structure and the chimney gas.

(v) Thermal properties of the solid layers are assumed independent of temperature.

(vi) The gas temperature is assumed uniform in any cross-section due to turbulent flow conditions. For the test chimney a typical entry Reynolds number is of the order of 6000.

(vii) The mass flow rate of the gas is assumed to be independent of temperature although it may vary with time, particularly in a cooling period.

(viii) For the purposes of simplification, the specific heat and density of the chimney gases are taken to be constant.

3.2. *Mathematical formulation of the problem*

3.2.1. *Differential equations for conduction in the chimney wall.* The unsteady state equation applies in each layer:

$$\frac{\partial \theta_j}{\partial t} = \alpha_j \frac{1}{r} \frac{\partial}{\partial r}\left(r \frac{\partial \theta_j}{\partial r}\right) \text{ for } j = 1, 2, 3 \qquad (1)$$

where $j = 1$ corresponds to the inner layer, $j = 2$ to the insulation and $j = 3$ to the outer layer. In the equation θ is temperature, α is thermal diffusivity, t is time and r is radial position.

3.2.2. *Boundary conditions for the solid.* The boundary conditions on the θ_j are:

$$-K_1 \frac{\partial \theta_1}{\partial r} = h_g(t)(\theta_g - \theta_1) \text{ at } r = r_1 \qquad (2)$$

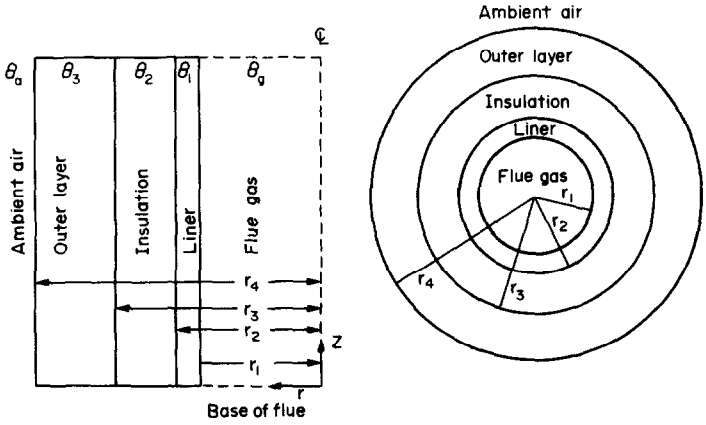

FIG. 3. Cross-section of a typical cylindrical three-dimensional chimney.

$$\left.\begin{aligned}\theta_{j-1} &= \theta_j \\ K_{j-1}\frac{\partial\theta_{j-1}}{\partial r} &= K_j\frac{\partial\theta_j}{\partial r}\end{aligned}\right\} \text{ at } r = r_j \text{ for } j = 2, 3 \tag{3, 4}$$

and

$$-K_3\frac{\partial\theta_3}{\partial r} = h_0(\theta_3 - \theta_a) \text{ at } r = r_4. \tag{5}$$

Equations (3) and (4) express the continuity of temperature and of heat flux at a solid interface on the assumption of perfect thermal contact. In these equations θ_g is the exhaust gas temperature, θ_a is the ambient air temperature, K is the thermal conductivity, and $h_g(t)$ and h_0 are the heat-transfer coefficients for the interfaces between the flue gas and liner and the outer layer and ambient air, respectively.

3.2.3. *Differential equation for the flue (exhaust) gas.* Assuming incompressible flow and constant heat capacity, the thermal energy balance for the gas can be written as:

$$\frac{\partial\theta_g}{\partial t} + u(t)\frac{\partial\theta_g}{\partial z} = -\frac{2h_g(t)}{\rho_g C_g r_1}\left[\theta_g - (\theta_1)_{r=r_1}\right] \tag{6}$$

where z is distance measured from the base of the chimney, ρ_g is the density of gas and C_g is its heat capacity per unit mass. u is the gas velocity, which at any instant is equal to

$$\frac{\dot{m}(t)}{\pi r_1^2 \rho_g}$$

where $\dot{m}$ is the mass flow rate of the gas.

Assuming incompressible flow, the continuity equation for the gas is:

$$\frac{\partial\dot{m}(t)}{\partial z} = 0. \tag{7}$$

This shows that the mass flow rate within the chimney is independent of position within the chimney. Hence $\dot{m}$ may be taken as the inlet mass flow rate, i.e.

$$\dot{m}(t) = \dot{m}_i(t). \tag{8}$$

The boundary condition on θ_g is:

$$\theta_g = \theta_i(t) \text{ at } z = 0. \tag{9}$$

Initial conditions The initial condition for the solid temperature is:

$$\theta_1 = \theta_2 = \theta_3 = \theta_a \tag{10}$$

for $z_f(t) \leqslant z \leqslant L$, $r_1 \leqslant r \leqslant r_4$ and $t \geqslant 0$, on the assumption that the whole of the chimney structure is initially at the ambient air temperature. This condition is a statement of the fact that the solid temperature cannot change until gas comes into contact with it, owing to the assumed lack of conduction in the z direction. $z_f(t)$ gives the position of the gas front on its first travel through the chimney.

The initial condition for the gas is:

$$\theta_g = \theta_i(0) \text{ at } z = 0 \text{ for } t = 0. \tag{11}$$

3.3. *Change to dimensionless variables*

The equations to be solved can be simplified by the following change of variables:

Dimensionless distance from the chimney base $= y = \varepsilon z$ (12)

Dimensionless time $= \tau = \beta(t - t_D)$ (13)

Dimensionless temperature $= \phi = \dfrac{\theta}{\theta_i(0)}$ (14)

Dimensionless radial distance $= R = \dfrac{r}{r_4}$ (15)

where t_D is the time taken by the fluid at height z at time t to travel from the chimney entrance to height z, and is given by the equation:

$$z = \int_{w=t-t_D}^{w=t} u(w)\,\mathrm{d}w = \frac{1}{\pi r_1^2 \rho_g}\int_{w=t-t_D}^{w=t} \dot{m}(w)\,\mathrm{d}w \tag{16}$$

and

$$\varepsilon = \frac{2h_g(0)}{r_1 \rho_g C_g u(0)} \tag{17}$$

and

$$\beta = \alpha_1 / r_4^2. \tag{18}$$

With these transformations, the differential equations to be solved (which are derived in Appendix 1) are as follows:

Equation (1) becomes:

$$\frac{\partial\phi_j}{\partial\tau} = F_1(y, \tau)\frac{\lambda_j}{R}\frac{\partial}{\partial R}\left(R\frac{\partial\phi_j}{\partial R}\right) \tag{19}$$

for $R_j \leqslant R \leqslant R_{j+1}$ $j = 1, 2, 3$, where

$$\lambda_j = \frac{\alpha_j}{\alpha_1} \text{ and } F_1(y, \tau) = \frac{\dot{m}(\tau/\beta)}{\dot{m}(t)}.$$

Equation (6) for the gas becomes:

$$\frac{\partial\phi_g}{\partial y} = -F_2(y, \tau)\left[\phi_g - (\phi_1)_{R=R_1}\right] \tag{20}$$

where

$$F_2(y, \tau) = \left\{\frac{\dot{m}(t)}{\dot{m}(0)}\right\}^{-0.2}$$

assuming $h_g \propto [\dot{m}(t)]^{0.8}$, (Dittius–Boelter equation [1]).

The corresponding dimensionless boundary and initial conditions are:

$$\frac{\partial\phi_1}{\partial R} = -F_3(y, \tau)\cdot B_g\cdot(\phi_g - \phi_1) \text{ at } R = R_1 \tag{21}$$

where

$$F_3(y, \tau) = \left\{\frac{\dot{m}(t)}{\dot{m}(0)}\right\}^{0.8} \text{ and } B_g = [h_g(0)r_4]/K_1$$

$$\left.\begin{aligned}\phi_{j-1} &= \phi_j \\ \frac{\partial\phi_{j-1}}{\partial R} &= \omega_j\frac{\partial\phi_j}{\partial R}\end{aligned}\right\} \text{ at } R = R_j \text{ for } j = 2, 3 \tag{22, 23}$$

where $\omega_j = K_j/K_{j-1}$

$$\frac{\partial\phi_3}{\partial R} = -B_0(\phi_3 - \phi_a) \text{ at } R = 1 \tag{24}$$

where $B_0 = h_0 r_4/K_3$, and

$$\phi_1 = \phi_2 = \phi_3 = \phi_a(0) \quad \text{at } \tau = 0 \text{ for } R_1 \leqslant R \leqslant 1 \text{ and } 0 \leqslant y \leqslant \varepsilon L \tag{25}$$

$$\phi_g = \phi_i(t) = \theta_i(t)/\theta_i(0) \text{ at } y = 0. \tag{26}$$

It should be noted that B_g and B_0 are Biot numbers for the inner and outer surfaces of the chimney, both based on the outer radius.

4. SOLUTION OF THE EQUATIONS

The equations are solved numerically by finite difference methods. A finite difference scheme for solving equations similar in form to those occurring in the present paper has been reported by Handley and Heggs [2].

4.1. *Gas temperature on the first pass*

As a first step in the numerical solution it is necessary to know the gas and solid temperatures at $\tau = 0$. Neglecting heat transfer from the chimney structure to (or from) the surrounding air (whose temperature varies) in the early stages, it can be assumed that the gas front encounters a liner temperature of $\theta_a(0)$ at each height, i.e.

$$(\theta_1)_{R=R_1} = \theta_a(0) \text{ at } z = z_f(t).$$

Now,

$$z_f(t) = \int_{w=0}^{w=t} u(w)\,\mathrm{d}w = \frac{1}{\pi r_1^2 \rho_g} \int_{w=0}^{w=t} \dot{m}(w)\,\mathrm{d}w$$

i.e. $t = t_D$ at the gas front.

This can be written in dimensionless form as:

$$(\phi_1)_{R=R_1} = \phi_a(0) \text{ at } \tau = 0.$$

therefore, at $\tau = 0$, equation (20) can be written:

$$\frac{\mathrm{d}}{\mathrm{d}y}(\phi_g)_{\tau=0} = F_2(y, 0)[\phi_a(0) - (\phi_g)_{\tau=0}].$$

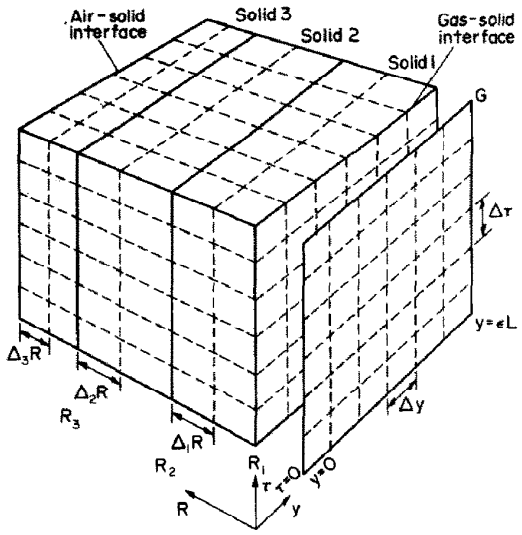

FIG. 4. Three-dimensional finite-difference grid system.

Integrating and using the condition that $(\phi_g)_{\tau=0} = 1$ at $y = 0$ gives:

$$(\phi_g)_{\tau=0} = \phi_a(0) + [1 - \phi_a(0)] \exp\left[- \int_{y=0}^{y=y} F_2(y, 0)\,\mathrm{d}y \right] \tag{27}$$

The corresponding solid temperatures are given by equation (25).

4.2. *The finite difference grid*

The solid temperature can be represented by a three dimensional grid, and the gas temperature by a two dimensional grid as shown in Fig. 4. The general temperatures at the grid points are:

$$\phi_g(y, \tau) = \phi_g(i\Delta y, n\Delta\tau)$$
$$\phi_1(R, y, \tau) = \phi_1[(R_1 + m_1\Delta_1 R), i\Delta y, n\Delta\tau]$$
$$\phi_2(R, y, \tau) = \phi_2[(R_2 + m_2\Delta_2 R), i\Delta y, n\Delta\tau]$$
$$\phi_3(R, y, \tau) = \phi_3[(R_3 + m_3\Delta_3 R), i\Delta y, n\Delta\tau].$$

4.3. *The finite difference equations*

4.3.1. *For the gas.* The finite difference form of equation (20) is:

$$\left[\frac{1}{\Delta y} + \frac{F_2(i-\tfrac{1}{2}, n+1)}{2}\right]\phi_g(i, n+1) - \frac{F_2(i-\tfrac{1}{2}, n+1)}{2}\phi_s(i, n+1)$$
$$= \left[\frac{1}{\Delta y} - \frac{F_2(i-\tfrac{1}{2}, n+1)}{2}\right]\phi_g(i-1, n+1) + \frac{F_2(i-\tfrac{1}{2}, n+1)}{2}\phi_s(i-1, n+1) \tag{28}$$

where $\phi_s(i, n+1) = \phi_1(0, i, n+1)$ is the inner liner temperature.

4.3.2. *Within the jth solid layer* ($j = 1, 2, 3$). Equation (19) can be expressed in the Crank–Nicholson [3] six-point implicit form about the point $[(R_j + m_j\Delta_j R), i\Delta y, (n+\tfrac{1}{2})\Delta\tau]$ as:

$$(1+2\gamma_j)\phi_j(m_j, i, n+1) - \gamma_j\left[1 + \frac{1}{2(\psi_j + m_j)}\right]\phi_j(m_j+1, i, n+1) - \gamma_j\left[1 - \frac{1}{2(\psi_j+m_j)}\right]\phi_j(m_j-1, i, n+1)$$
$$= (1-2\gamma_j)\phi_j(m_j, i, n) + \gamma_j\left[1 + \frac{1}{2(\psi_j+m_j)}\right]\phi_j(m_j+1, i, n) + \gamma_j\left[1 - \frac{1}{2(\psi_j+m_j)}\right]\phi_j(m_j-1, i, n) \tag{29}$$

for $1 \leqslant m_j \leqslant M_{j-1}$

where $M_j = (R_{j+1} - R_j)/\Delta_j R$

$\gamma_j = \lambda_j F_1(i, n+\tfrac{1}{2})\Delta\tau/2(\Delta_j R)^2$

$\psi_j = R_j/\Delta_j R.$

The derivation of the finite difference forms of the boundary conditions, which are given below, can be found in Appendix 2.

4.3.3. *At the interface between the* $(j-1)$*th and* j*th solids* $(j = 2, 3)$. The continuity of temperature conditions [equation (22)] become:

$$\phi_{j-1}(M_{j-1}, i, n+1) = \phi_j(0, i, n+1) \tag{30}$$

$$\phi_{j-1}(M_{j-1}, i, n) = \phi_j(0, i, n) \tag{31}$$

and the continuity of flux condition [equation (23)] can be expressed for $(n+\frac{1}{2})\Delta\tau$ as:

$$\left\{\frac{(1+2\gamma_{j-1})}{\gamma_{j-1}\left[1+\dfrac{1}{2(\psi_{j-1}+M_{j-1})}\right]\Delta_{j-1}R} + \frac{\omega_j(1+2\gamma_j)}{\gamma_j\left(1-\dfrac{1}{2\psi_j}\right)\Delta_j R}\right\}\phi_j(0, i, n+1)$$

$$- \frac{2\omega_j\phi_j(1, i, n+1)}{\left(1-\dfrac{1}{2\psi_j}\right)\Delta_j R} - \frac{2\phi_{j-1}(M_{j-1}-1, i, n+1)}{\left[1+\dfrac{1}{2(\psi_{j-1}+M_{j-1})}\right]\Delta_{j-1}R}$$

$$= \left\{\frac{(1-2\gamma_{j-1})}{\gamma_{j-1}\left[1+\dfrac{1}{2(\psi_{j-1}+M_{j-1})}\right]\Delta_{j-1}R} + \frac{\omega_j(1-2\gamma_j)}{\gamma_j\left(1-\dfrac{1}{2\psi_j}\right)\Delta_j R}\right\}\phi_j(0, i, n)$$

$$+ \frac{2\omega_j\phi_j(1, i, n)}{\left(1-\dfrac{1}{2\psi_j}\right)\Delta_j R} + \frac{2\phi_{j-1}(M_{j-1}-1, i, n)}{\left[1+\dfrac{1}{2(\psi_{j-1}+M_{j-1})}\right]\Delta_{j-1}R}. \tag{32}$$

4.3.4. *At the gas–liner interface.* Equation (21) can be written in finite difference form as:

$$\frac{2}{\left(1-\dfrac{1}{2\psi_1}\right)\Delta_1 R}\phi_1(1, i, n+1) - \left[\frac{(1+2\gamma_1)}{\gamma_1\left(1-\dfrac{1}{2\psi_1}\right)\Delta_1 R} + 2\eta\right]\phi_s(i, n+1) + 2\eta\phi_g(i, n+1)$$

$$= \frac{-2\phi_1(1, i, n)}{\left(1-\dfrac{1}{2\psi_1}\right)\Delta_1 R} - \left[\frac{(1-2\gamma_1)}{\gamma_1\left(1-\dfrac{1}{2\psi_1}\right)\Delta_1 R} - 2\eta\right]\phi_s(i, n) - 2\eta\phi_g(i, n) \tag{33}$$

where $\phi_1(0, i, n+1)$ and $\phi_1(0, i, n)$ have been replaced by $\phi_s(i, n+1)$ and $\phi_s(i, n)$ respectively and where $\eta = F_3(i, n+\frac{1}{2})B_g$.

4.3.5. *At the outer layer–air interface.* The boundary condition [equation (24)] can be replaced in finite difference form by:

$$\left\{\frac{(1+2\gamma_3)}{\gamma_3\left[1+\dfrac{1}{2(\psi_3+M_3)}\right]\Delta_3 R} + 2B_0\right\}\phi_3(M_3, i, n+1) - \frac{2\phi_3(M_3-1, i, n+1)}{\left[1+\dfrac{1}{2(\psi_3+M_3)}\right]\Delta_3 R}$$

$$= \left\{\frac{(1-2\gamma_3)}{\gamma_3\left[1+\dfrac{1}{2(\psi_3+M_3)}\right]\Delta_3 R} - 2B_0\right\}\phi_3(M_3, i, n) + \frac{2\phi_3(M_3-1, i, n)}{\left[1+\dfrac{1}{2(\psi_3+M_3)}\right]\Delta_3 R} + 4B_0F_4(i, n+\tfrac{1}{2}) \tag{34}$$

where $F_4(y, \tau) \equiv \phi_a(z, t)$.

Equations (28), (29), (32)–(34) are a set of $(M_1+M_2+M_3+2)$ linear simultaneous equations in the $(M_1+M_2+M_3+2)$ unknown temperatures at $i\Delta y$, $(n+1)\Delta\tau$. These temperatures are:

$\phi_3(m_3, i, n+1)$, $0 \leqslant m_3 \leqslant M_3$
$\phi_2(m_2, i, n+1)$, $0 \leqslant m_2 \leqslant M_{2-1}$
$\phi_1(m_1, i, n+1)$, $1 \leqslant m_1 \leqslant M_{1-1}$
$\phi_s(i, n+1)$
$\phi_g(i, n+1)$.

5. SOLUTION PROCEDURE

The gas and solid temperatures at any position and time are calculated from the known temperatures at $\tau = 0$ in the following way. For the first time step $\tau = \Delta\tau$, equations (29), (32)–(34) are solved at the base of the chimney $i = 0$. Then equations (28), (29)–(34) are solved for each chimney height step for the first time step. The procedure is then repeated for each time step.

5.1. *Input quantities required by the computer program*

The computer program simulates the three layer experimental chimney (Fig. 1) and the following quantities are required as input data for the program:

$\dot{m} = \dot{m}(t)$ = mass flow rate of gases through the chimney as a function of time for both heating and cooling periods:

h_g = inside heat-transfer coefficient for both periods;
h_0 = outside heat-transfer coefficient;
ρ_g, C_g, = density and specific heat of gases for both periods (these are based on the average inlet temperature for the period under consideration);
K_1, K_2, K_3 = thermal conductivity of each of the three chimney layers;
ρ_1, ρ_2, ρ_3 = density of each layer;
C_1, C_2, C_3 = specific heat of the three chimney layers;
r_1, r_2, r_3 = inner radius of each layer;
r_4 = outer radius of chimney;
θ_A = cooling air temperature as a function of time and chimney height;

and the curve of chimney inlet gas temperature vs time for both heating and cooling periods.

In the test apparatus (Fig. 1) the mass flow rate was kept constant for the heating period but varied during the cooling period. Time is measured from the beginning of the heating period and the solid and gas temperatures are calculated for each time step until the end of the heating period is reached. In the transition period, i.e. in the change from heating to cooling, the exhaust gases are being replaced by cooling air in practice and the program assumes that the exhaust gas is replaced instantaneously with air, which assumes the temperature of the gas it replaces. The error in such an assumption is very small since the time of the travel of gases up the experimental chimney for the heating period is

$$\frac{L}{u} = \frac{L\pi r_1^2 \rho_g}{\dot{m}} = 1.6\,\text{s}$$

compared with the time step in the computer program which was set at 30 s.

The cooling period is calculated in exactly the same way as a heating period. Time is measured afresh and the solid and gas temperatures calculated at the end of the heating period provide the starting values for the cooling period. A new inlet flue gas transient, mass flow rate of air $[\dot{m}(t)]$ and heat-transfer coefficient $[h_g(t)]$, are required for the residual gas flow. It should be observed that the grid will also change for the cooling period—it will either stretch or contract at the instant of changeover. Whilst Δz—the actual chimney height step—remains fixed, the dimensionless height steps (Δy) during a heating and a cooling period are given by:

$$\Delta y_H = \varepsilon_H \Delta z \text{ and } \Delta y_C = \varepsilon_C \Delta z \text{ respectively,}$$

where

$$\varepsilon_H = \left[\frac{2h_g(0)}{r_1 \rho_g C_g u(0)}\right]_H \text{ and } \varepsilon_C = \left[\frac{2h_g(0)}{r_1 \rho_g C_g u(0)}\right]_C$$

and where the subscripts H and C refer to the heating and cooling periods respectively.

At the end of a cooling period, the program assumes that the air is replaced instantaneously by the exhaust gases for the new heating period, the exhaust gases

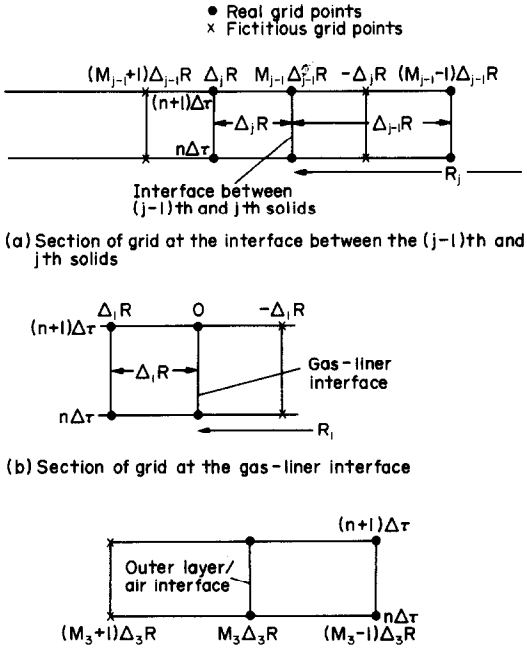

FIG. 5. (a) Section of the finite difference grid at the interface between the $(j-1)$th and jth solids. (b) Section of the finite difference grid at the gas–liner interface. (c) Section of the finite difference grid at the interface between the outer chimney layer and the ambient air.

taking on the temperatures of the air. In this case a typical time taken for the cooling gases to pass through the chimney is

$$\frac{L}{u} = \frac{L\pi r_1^2 \rho_g}{\dot{m}} = 7.2\,\text{s}$$

compared with a time step of $\Delta t = 30$ s.

Thus the program can predict heating and cooling periods and consequently complete cycles. It is the behaviour of the chimney under cycling conditions which is of particular interest to the heating engineer and so the facility of plotting the inside chimney temperature transients (for complete cycles) was incorporated into the program (see Fig. 6).

5.2. *Accuracy of the computer solution*

The stability of the equations is enhanced by their implicit nature—in particular the use of the Crank–Nicholson [3] finite difference formula.

The convergence and accuracy of the numerical solution obviously depend on the values chosen for $\Delta_1 R, \Delta_2 R, \Delta_3 R$. Δy and $\Delta\tau$ (see discussion by Handley and Heggs [2]). The values chosen should give a reasonable compromise between accuracy and computing time.

Table 1 shows the effect on the calculated solid and gas temperatures of varying the time step Δt from 1 to 60 s. Table 2 shows the effect on the calculated inner liner temperature of varying the height step (Δz) from 0.5 to 2 ft, keeping $\Delta t = 30$ s. These predictions apply to the six feet test section of the experimental chimney shown in Fig. 1.

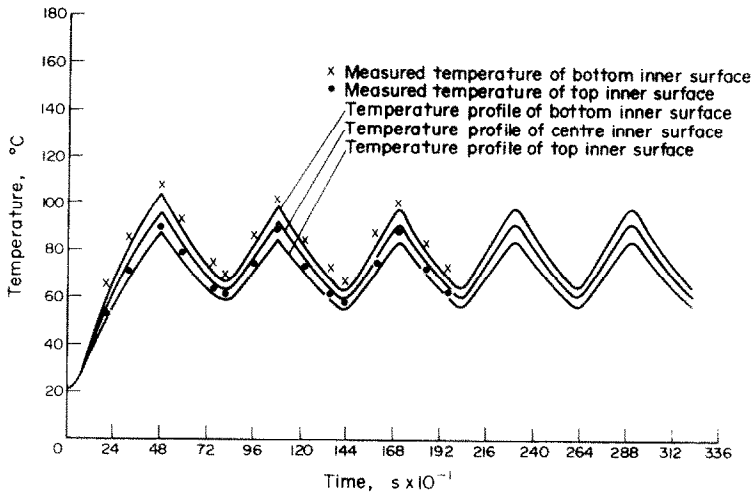

FIG. 6. Computer plot of a cycling test.

Table 1. Variation of predicted liner and gas temperatures for different time steps
The height step $\Delta z = 1$ ft.
The predicted temperatures are those after 60 s.

Δt (s)	Inner liner base temperature (°C)	Gas temperature at chimney exit (°C)
1	25.05	32.99
5	25.04	32.98
30	24.96	32.97
60	24.86	32.95

Table 2. Variation of chimney liner temperature for two different height steps
The time step $\Delta t = 30$ s.
The predicted temperatures are those after 60 s.

Δz (ft)	Inside chimney liner at a height of 4 ft (°C)
0.5	61.74
2.0	61.73

For the experimental chimney under consideration in Fig. 1, all predicted temperatures for the above time and height steps are within 0.5°C of each other at corresponding heights and times.

All computer calculations were done on the UNIVAC 1108 computer. A typical heating and cooling cycle of 40 min at $\Delta t = 30$ s and $\Delta z = 1$ ft took 7.8 s computing time, the number of different temperature predictions being 9600.

6. COMPARISON OF THEORETICAL PREDICTIONS WITH EXPERIMENTAL VALUES

The quantities measured by DOBETA on the experimental chimney (Section 2) permitted the calculation of the input data for the program (Section 5.1). The heat-transfer coefficients h_g and h_0 were calculated from the standard formula of Dittius–Boelter [1], averaged over the temperature range involved. In the case of h_0, the convective flow rates in the test apparatus were so great that the radiative contribution could be neglected by comparison. The values of C_g and ρ_g were the average of their values evaluated at the initial and ultimate inlet gas temperatures in any period. The thermal properties of all the three layers were obtained from tables with the exception of the thermal conductivity of vermiculite which was obtained from steady state measurements on the apparatus. In the cooling period, $\dot{m}$ and consequently h_g were calculated from measurements of the residual gas flow velocity.

Six separate tests were carried out by DOBETA. For three tests (A, B and C) the boiler was switched on for about 30 min so that temperatures were steady before cooling down. A different firing rate and quantity of excess air was used in each case. These three tests are tabulated in Table 3.

Table 3.

Test	Firing rate (kg/s)	Carbon dioxide concentration in exhaust chimney gases (%)	Maximum inlet (°C) exhaust temperature
A	9.6×10^{-4}	12.6	350
B	6.0×10^{-4}	8.1	350
C	6.3×10^{-4}	8.8	350

Figures 7–9 show the comparison between the predicted and experimental temperatures for each of the three tests A, B and C taken over a complete cycle. The curves show the predicted and measured outlet flue gas temperatures and top inner skin temperature as functions of time. These three curves show that predicted temperatures and measured temperatures were within 10% of each other over most of the range. The predictions for all the tests were similar in accuracy. Measured and predicted outer surface temperatures were also found to be in good agreement. However, as the primary purpose of the model is to predict inner liner temperatures, which govern condensation, this comparison has not been shown.

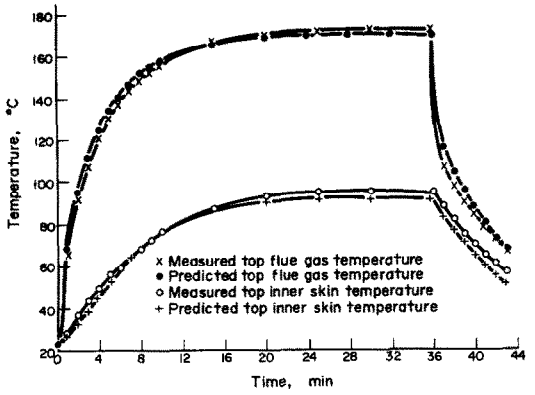

FIG. 7. Comparison of predicted and measured temperatures—Test *A*. (Firing rate = 57.7 g/min.)

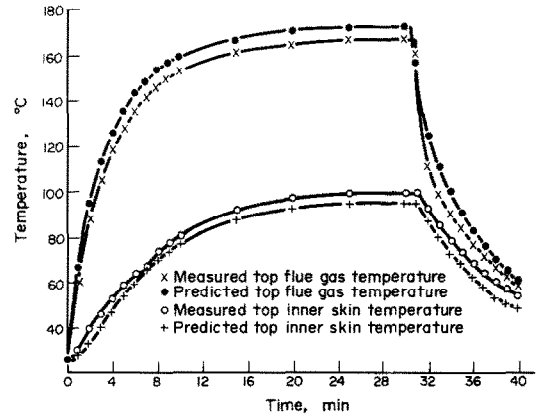

FIG. 8. Comparison of predicted and measured temperatures—Test *B*. (Firing rate = 36.0 g/min.)

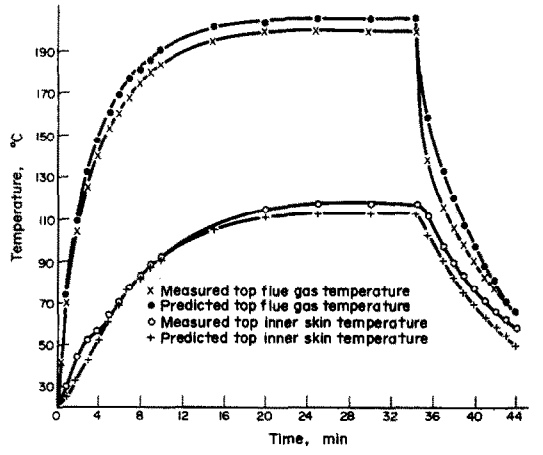

FIG. 9. Comparison of predicted and measured temperatures—Test *C*. (Firing rate = 37.6 g/min.)

Figure 6 shows a computer plot of a cycling test for five consecutive cycles. This corresponds to test A under cycling conditions. Its usefulness in predicting the tendency to water and acid condensation can be clearly seen by taking the water dewpoint temperature as 45°C and the acid dewpoint temperature as 140°C. Under these boiler cycling conditions, and with this design of chimney, it can be seen that the chimney suffers from water condensation for only 200 s in the first heating period. All the inner liner temperatures are below the acid dewpoint at all times and extensive acid condensation can be anticipated.

Concerning Figs. 7–9, an interesting observation is that during the early part of the heating period, the gradient of the measured values of inner skin temperatures suddenly rises and falls again, whereas the predicted gradients have a smooth slope. This could be due to latent heat effects as this observation occurs when the wall temperature is about 50–70°C. Thus it might be suspected that of the heat passing from the gas to the surface, a high proportion will cause the water to change its state into gas and so the temperature of the metal will not rise so rapidly at that point. This would not be predicted theoretically as no account has been taken of the effect of condensation on the heat transfer. This observation is not apparent in the cooling cycle, because only air is passing through the chimney and it contains only ambient moisture. Thus there is negligible condensation in a cooling period by comparison with a heating period.

7. MODIFICATIONS FOR A PRACTICAL CHIMNEY

A practical chimney is sometimes of square cross section with a cylindrical liner. To simplify the mathematical treatment, the actual cross section can be replaced by an equivalent three layer circular section (liner, insulation, outer layer), with the radii chosen so that each layer contains the same amount of the material as the actual chimney. Here the assumption is that the mass of the layer (which governs its thermal capacity) is more important than its surface area.

The outer face of a practical chimney may lose heat by a considerable amount of radiation as well as convection. The existing model can still be applied by combining both the heat loss processes as a linearized heat loss law for the outer face.

The ambient air temperature will be a function of time alone and independent of chimney height for a practical chimney.

It must be emphasised that to predict the thermal performance of any chimney design, a typical cycle for mass flow rate and temperature at the base of the chimney must be known in advance. A qualitative indication of the variation with time of flow in a practical domestic boiler/chimney system is shown in Fig. 10.

7.10. *Evaluation of* t *as a function of* y *and* τ *when* $\dot{m}(t)$ *is given in graphical or tabular form for any period*

Since in practice the mass flow rate $\dot{m}(t)$ may be given in graphical or tabular form (cf. Fig. 10), it is convenient to tabulate t as a function of y and τ and hence F_1, F_2 and F_3 as functions of y and τ. These calculations are performed prior to the beginning of the finite difference solutions. In the finite difference solution, the temperatures are calculated at all points for $\tau = \Delta\tau$ given starting values at $\tau = 0$. The procedure is then repeated for $\tau = 2\Delta\tau$, $3\Delta\tau$ etc. Hence values of t must be calculated for each value of y ($= i\Delta y$ where

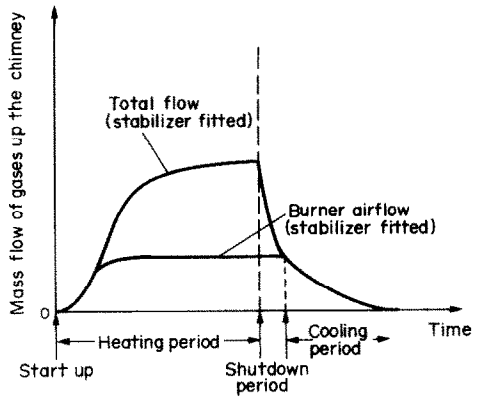

FIG. 10. Qualitative variation with time of mass flow in a boiler (burner) chimney system.

$0 \leqslant i \leqslant I$) at a given τ ($=n\Delta\tau$ where $0 \leqslant n \leqslant N_1$). The procedure is as follows:

(i) Equation (16) can be written in the form:

$$z = A(t) - A(t - t_D)$$

where

$$A(t) = \frac{1}{\pi r_1^2 \rho_g} \int_{w=0}^{w=t} \dot{m}(w)\,\mathrm{d}w.$$

(ii) A table of values of $A(t)$ vs t can be drawn up for $t = n\Delta t$, $0 \leqslant n \leqslant N_1$. This can be achieved by numerical integration using the graphical or tabular values of $\dot{m}(t)$ vs t.

(iii) For one value of $\tau = n\Delta\tau$,

$$t - t_D = \frac{\tau}{\beta} = n\frac{\Delta\tau}{\beta}.$$

From the $A(t)$ vs t table, the value of $A(n\Delta\tau/\beta)$ can be found by interpolation. For one value β of $y = i\Delta y$, $z = i\Delta y/z$ and since $a(t) = z + A(t - t_D)$, this gives a value for $A(t)$. From the table of $A(t)$ vs t the corresponding value of t can be found. Hence t for the chosen y. The calculation is repeated for all y values in the mesh to give a table of values of t vs y for all y values on the mesh for the fixed value of τ.

(iv) Stage (iii) is repeated for all τ values on the mesh. A series of tables of t vs y can thus be obtained for all τ values.

(v) Since t is now known in terms of y for all τ values, F_1, F_2 and F_3 can be calculated and tables of values of F_1, F_2 and F_3 vs y for each value of τ can be produced.

It should be noted that after the first few values of $\Delta\tau$ in any time period, t_D will be very much less than t, and hence after the first few $\Delta\tau$, $t \doteq \tau/\beta$.

Then

$$F_1(y, \tau) \doteq 1$$

$$F_2(y, \tau) \doteq \left\{\frac{\dot{m}(0)}{\dot{m}(\tau/\beta)}\right\}^{0.2}$$

$$F_3(y, \tau) \doteq \left\{\frac{\dot{m}(\tau/\beta)}{\dot{m}(0)}\right\}^{0.8}$$

thus eliminating the need to obtain tabular values of F_1, F_2 and F_3 as in steps (i)–(v) for more than the first few time steps.

8. CONCLUSIONS

The mathematical model for prediction of temperatures in a multilayer chimney under the unsteady state conditions encountered with variable flue gas inlet conditions and variable ambient temperature has been successfully compared with measurements on an experimental chimney. For known acid and water dewpoint temperatures for the chimney gases, a realistic forecast can be made of the time period for which any part of the chimney liner is subject to acid and water condensation. In consequence the model can be used to aid the selection of chimney designs and the identification of boiler operating conditions which will minimize low temperature corrosion resulting from the formation of condensates within the chimney.

The model should find wide application, particularly in oil fired installations where acid and water condensation can seriously limit the life of a chimney.

Following the present verification of the model, it is intended to utilize it for the production of design curves for practical chimney/boiler systems which will lead to minimum condensation.

Acknowledgement—The authors wish to thank research staff at Shell Research Ltd./Egham Research Laboratories for valuable advice and ideas throughout the project. Particular thanks are due to Mr. George Milburn for his assistance in writing the computer program.

REFERENCES

1. W. McAdams, Review and summary of developments in heat transfer by conduction and convection, *Trans. Am. Instn Chem. Engrs* **36**, 1 (1940).
2. D. Handley and P. J. Heggs, The effect of thermal conductivity of the packing material on transient heat transfer in a packed bed, *Int. J. Heat Mass Transfer* **12**, 549–570 (1969).
3. J. Crank and P. Nicholson, A practical method for numerical evaluation of solutions of partial differential equations of the heat conduction type, *Proc. Camb. Phil. Soc.* **43**, 50–67 (1947).

APPENDIX 1

Derivation of the Dimensionless Differential Equations for the Case when the Inlet Mass Flow Rate Varies with Time

In equation (16) t_D is defined as the time taken by the fluid at height z and time t to travel from the chimney entrance to height z.

$$z = \frac{1}{\pi r_1^2 \rho_g} \int_{w=t-t_D}^{w=t} \dot{m}(w)\,\mathrm{d}w = g(t, t_D) \text{ say.} \qquad (16)$$

Suppose it is required to find $\partial G/\partial t$ and $\partial G/\partial z$ given a function $F(z, t) = G(y, \tau)$. Using equations (12) and (13), since β and ε are independent of t and z.

$$\frac{\partial G}{\partial t} = \beta\left(1 - \frac{\partial t_D}{\partial t}\right)\frac{\partial G}{\partial \tau} \quad \text{and} \quad \frac{\partial G}{\partial z} = -\beta\frac{\partial t_D}{\partial z}\cdot\frac{\partial G}{\partial \tau} + \varepsilon\frac{\partial G}{\partial y}.$$

To find the partial derivatives of t_D the result

$$\frac{\partial}{\partial y}\left[\int_{a(Y,z)}^{b(Y,z)} g(x, Y, z)\,\mathrm{d}x\right] = \int_a^b \frac{\partial g}{\partial Y}\cdot\mathrm{d}x + g(b, Y, z)\cdot\frac{\partial b}{\partial Y} - g(a, Y, z)\frac{\partial a}{\partial Y}$$

is used.

Differentiating (16) partially with respect to z and t and using the above result, we have:

$$\frac{\partial t_D}{\partial z} = \frac{1}{u(t-t_D)} \text{ and } \frac{\partial t_D}{\partial t} = 1 - \frac{u(t)}{u(t-t_D)}.$$

Hence

$$\frac{\partial G}{\partial t} = \beta \frac{u(t)}{u(t-t_D)} \frac{\partial G}{\partial \tau} \tag{A1}$$

and

$$\frac{\partial G}{\partial z} = \varepsilon \frac{\partial G}{\partial y} - \left[\frac{\beta}{u(t-t_D)}\right] \frac{\partial G}{\partial \tau}. \tag{A2}$$

Using results (A1) and (A2), dividing through by $\theta_i(0)$, and substituting for ε from (17) reduces (6) to the form

$$\frac{\partial \phi_g}{\partial y} = -\left[\frac{\dot{m}(t)}{\dot{m}(0)}\right]^{-0.2} [\phi_g - (\phi_1)_{R=R_1}]. \tag{20}$$

This is the dimensionless equation for the gas in the text.

The differential equation for any solid layer is:

$$\partial \theta_j / \partial t = \alpha_j \frac{1}{r} \frac{\partial}{\partial r}\left(r \frac{\partial \theta_j}{\partial r}\right) \text{ for } j = 1, 2, 3. \tag{1}$$

Using result (A1) and putting

$$\beta = \frac{\alpha_1}{r_4^2} \tag{18}$$

equation (1) becomes:

$$\frac{\partial \phi_j}{\partial \tau} = \lambda_j \left[\frac{\dot{m}(t-t_D)}{\dot{m}(t)}\right] \frac{1}{R} \frac{\partial}{\partial R}\left(R \frac{\partial \phi_j}{\partial R}\right) \tag{19}$$

where $\lambda_j = \alpha_j/\alpha_1$. This is equation (19) in the text.

APPENDIX 2

Expression of the Boundary Conditions in Finite Difference Form

At the interface between the (j − 1)*th and* j*th solids* (j = 2, 3)

The relevant section of the grid is shown in Fig. 5(a). At the interface in the $(j-1)$th layer, the finite difference equation within the solid can be applied if the $(j-1)$th solid is assumed to be on both sides of the interface. The equation is from [equation (29)]:

$$\begin{aligned}(1+2\gamma_{j-1})\phi_{j-1}(M_{j-1}, i, n+1) &- \gamma_{j-1}\left[1+\frac{1}{2(\psi_{j-1}+M_{j-1})}\right]\phi^*_{j-1}(M_{j-1}+1, i, n+1) \\ &- \gamma_{j-1}\left[1-\frac{1}{2(\psi_{j-1}+M_{j-1})}\right]\phi_{j-1}(M_{j-1}-1, i, n+1) \\ = (1-2\gamma_{j-1})\phi_{j-1}(M_{j-1}, i, n) &+ \gamma_{j-1}\left[1+\frac{1}{2(\psi_{j-1}+M_{j-1})}\right]\phi^*_{j-1}(M_{j-1}+1, i, n) \\ &+ \gamma_{j-1}\left[1-\frac{1}{2(\psi_{j-1}+M_{j-1})}\right]\phi_{j-1}(M_{j-1}-1, i, n)\end{aligned} \tag{A3}$$

where the temperatures marked with an asterisk are fictitious temperatures at the fictitious grid points in the extended $(j-1)$th solid.

At the same interface in the jth solid (assuming solid j material on both sides of the interface) the equation is:

$$\begin{aligned}(1+2\gamma_j)\phi_j(0, i, n+1) &- \gamma_j\left(1+\frac{1}{2\psi_j}\right)\phi_j(1, i, n+1) - \gamma_j\left(1-\frac{1}{2\psi_j}\right)\phi^*_j(-1, i, n+1) \\ &= (1-2\gamma_j)\phi_j(0, i, n) + \gamma_j\left(1+\frac{1}{2\psi_j}\right)\phi_j(1, i, n) + \gamma_j\left(1-\frac{1}{2\psi_j}\right)\phi^*_j(-1, i, n).\end{aligned} \tag{A4}$$

The continuity conditions at the interface are:

$$\phi_{j-1} = \phi_j \text{[equation (22)]} \quad \text{and} \quad \frac{\partial \phi_{j-1}}{\partial R} = \omega_j \frac{\partial \phi_j}{\partial R} \text{[equation (23)]}.$$

The continuity of temperature conditions are:

$$\phi_{j-1}(M_{j-1}, i, n+1) = \phi_j(0, i, n+1)$$
$$\phi_{j-1}(M_{j-1}, i, n) = \phi_j(0, i, n).$$

The continuity of flux condition can be written for $(n+\frac{1}{2})\Delta\tau$ as:

$$\begin{aligned}\tfrac{1}{2}\left\{\frac{[\phi^*_{j-1}(M_{j-1}+1, i, n+1) - \phi_{j-1}(M_{j-1}-1, i, n+1)]}{2\Delta_{j-1}R} + \frac{[\phi^*_{j-1}(M_{j-1}+1, i, n) - \phi_{j-1}(M_{j-1}-1, i, n)]}{2\Delta_{j-1}R}\right\} \\ = \frac{w_j}{2}\left\{\frac{[\phi_j(1, i, n+1) - \phi^*_j(-1, i, n+1)]}{2\Delta_j R} + \frac{[\phi_j(1, i, n) - \phi^*_j(-1, i, n)]}{2\Delta_j R}\right\}\end{aligned} \tag{A5}$$

Elimination of the fictitious temperatures between (A3), (A4) and (A5), followed by rearrangement, gives equation (32) in Section 5.3.3.

At the gas/liner and outer layer/liner interfaces

The relevant sections of the grid for the gas/liner interface and the outer layer/air interface are shown in Figs. 5(b) and 5(c) respectively. The final finite difference equations (33) and (34) are obtained in a similar manner by elimination of the fictitious temperatures.

CALCUL DES TEMPERATURES D'UNE CHEMINEE MULTICOUCHE DANS DES CONDITIONS DE REGIME VARIABLE

Résumé—On présente un modèle mathématique pour prédire la température en un point quelconque d'une cheminée multicouche dans des conditions instationnaires avec une température d'entrée et un débit de gaz variables et aussi une température ambiante variable. Le modèle redonne de façon satisfaisante les températures mesurées sur une cheminée expérimentale à trois couches, à la fois dans les périodes de chauffage et de refroidissement. En particulier, le modèle détermine correctement la période de temps pendant laquelle une portion quelconque de la zone interne est au dessous de la température du point de rosée acide des fumées. On peut réduire sensiblement la condensation de l'acide et de l'eau ainsi que la corrosion dans les cheminées en minimisant ce temps par des modifications dans la conception d'une cheminée domestique et des conditions opératoires sur la chaudière.

DIE ERMITTLUNG DER WANDTEMPERATUREN EINES MEHRSCHICHTIGEN KAMINS UNTER INSTATIONÄREN BEDINGUNGEN

Zusammenfassung—Es wird ein mathematisches Modell vorgestellt, das die Berechnung der Temperaturen an jedem Punkt eines mehrschichtigen Kamins unter instationären Bedingungen, wie sie bei variablen Rauchgaseintrittstemperaturen und Rauchgasmengenströmen, sowie variablen Umgebungstemperaturen anzutreffen sind, erlaubt. Die in einem dreischichtigen Versuchskamin über die Heiz- und Kühlperioden gemessenen Temperaturen wurden mit Hilfe dieses Modells in befriedigender Weise vorausberechnet. Insbesondere gibt das Modell korrekt die Zeitspanne, während der die innere Oberflächentemperatur an jeder Stelle des Kamins unter den Säure- und Wassertaupunkttemperaturen des Rauchgases liegt. Diese Zeit lässt sich durch Modifikationen in Wohnhauskaminen und in den Kesselbetriebsbedingungen zu einem Minimum machen, wodurch die Gefahr der Säure- und Wasserkondensation und der damit verbundenen Kaminkorrosion erheblich vermindert wird.

РАСЧЕТ ТЕМПЕРАТУР МНОГОСЛОЙНОЙ ОБШИВКИ ТРУБЫ В СТАЦИОНАРНЫХ УСЛОВИЯХ

Аннотация — Представлена математическая модель, которую можно использовать для расчета температуры в любой точке многослойной трубы в нестационарных условиях с переменной температурой на входе и переменным массовым расходом газов, а также переменной температурой окружающей среды. Модель удовлетворительно предсказывает значения температуры, измеренные в трехслойной экспериментальной трубе как в периоды нагревания, так и при охлаждении. В частности, с помощью данной модели можно точно определить период времени, в течение которого на любом участке внутренней обшивки трубы температура газов ниже точки росы для кислоты и воды. Уменьшая этот период путем некоторых изменений в конструкции труб, используемых в бытовых целях, и изменении режимов работы бойлеров, можно значительно снизить конденсацию кислоты и воды, а, следовательно, и коррозию трубы.